ACS Photonics

Article

pubs.acs.org/journal/apchd5

Sensitivity of Interferometric Cross-Polarization Microscopy for Nanoparticle Detection in the Near-Infrared

Benjamin T. Miles,[†] Elizabeth C. Robinson,[†] Erik M. H. P. van Dijk,[‡] Ian D. Lindsay,[†] Niek F. van Hulst,[§,∥] and Henkjan Gersen*[,†]

[†]Nanophysics and Soft Matter Group, H.H. Wills Physics Laboratory, University of Bristol, Bristol, BS8 1TL, United Kingdom

[‡]Faculty of Science and Technology, University of Twente, 7500 AE Enschede, The Netherlands

[§]ICFO - Institut de Ciencies Fotoniques, 08860 Castelldefels (Barcelona), Spain

[∥]ICREA - Institució Catalana de Recerca i Estudis Avançats, 08010 Barcelona, Spain

ABSTRACT: We address the sensitivity of Interferometric Cross-Polarization Microscopy by comparing scattering and absorption by spherical 10 nm nanoparticles through a combination of modeling and experiment. We show that orthogonality of light in the two polarization branches of Cross-Polarization Microscopy ensures that only light that has interacted with a nanoparticle is interferometrically enhanced. As a result background-free shot noise-limited detection is achieved for sub-μW optical powers at the sample. Our modeling in particular shows that in the near-infrared regime, above the plasmon resonance frequency of spherical nanoparticles, the cross-polarization approach is several orders of magnitude more sensitive than conventional extinction based detection. This enhanced near-infrared sensitivity for spherical nanoparticles is promising for applications requiring low absorption and low power imaging of nanoparticles in cells.

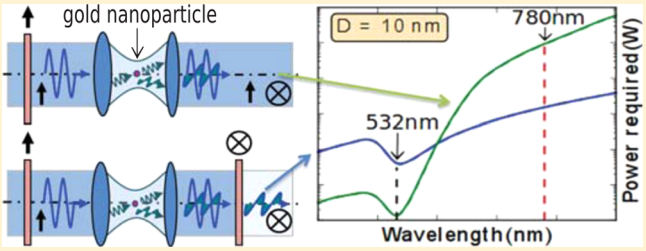

KEYWORDS: *confocal microscopy, nanoparticle detection, Mie scattering, cross-polarization imaging, gold nanoparticles, background free detection, detection sensitivity*

Inside the living cell, a multitude of dynamic processes occur, which are routinely studied by a large variety of biological and physical methods based on detection of single fluorescent molecules.[1] For example, the detection of fluorescent labels, or autofluorescence from proteins, is used to track the conformation, position and movement of proteins, filaments, and DNA, both in vitro and in vivo.[2−4] Moreover, the photophysical dynamics of the fluorophore, such as fluorescence lifetime and energy transfer, directly reports on the local nanoenvironment.[5] Clearly the detection of single fluorophores for nanoscale bioimaging has found a wide range of applications, as confirmed by the 2014 Nobel prize.[6] Yet the reliance on fluorescence is accompanied by a number of limitations. First, organic molecules do convert to a non-fluorescent state after a limited number of photocycles, which limits the observation time of the experiment and simultaneously induces phototoxicity.[7] Second, the finite lifetime of the excited state results in saturation, which limits the maximum emitted intensity and, thereby, the precision and time resolution with which individual fluorophores can be tracked.[8]

An attractive alternative to fluorescent labels that does not suffer from the above limitations is provided by metallic nanoparticles, which are already widely used in biology for single particle tracking and localization.[9] The optical signal from these particles is strong, very stable and does not suffer from photobleaching. Moreover, as the scattered signal from these nanoparticles is proportional to the incident intensity, the limitation on achievable time resolution is removed as the arrival rate of scattered photons can be enhanced by increasing the incident intensity.[8] To operate at this higher intensity it is advantageous to work in the near-infrared regime (NIR) where absorption by water and biomolecules is minimal, which, combined with lower photon energies, substantially reduces phototoxicity.[1,10] However, to follow biological processes it is paramount that the label used is small compared to the molecular machinery inside the cell, typically a few tens of nanometers in size.[1] Detecting nanoscale objects in the 10 nm size regime is challenging, as their cross-section is small, typically limiting the detection to particles with a diameter larger than ∼30 nm in conventional microscopy.[1,11]

The clear potential for biological applications has triggered the development of a variety of optical approaches to detect individual nanoparticles smaller than ∼30 nm, as recently reviewed in depth by Yurt et al.[12] as well as Zijlstra and Orrit.[11] Several of these approaches have now even demonstrated the detection of a single molecule in absorption, convincingly demonstrating the sensitivity that can be achieved.[13−16] However, a drawback to nearly all of these approaches is that

Received: June 12, 2015
Published: November 3, 2015

DOI: 10.1021/acsphotonics.5b00326
ACS Photonics 2015, 2, 1705−1711

they are resonant and require high optical powers incident on the sample at the wavelengths where absorption by biomolecules is large, which is prone to induce photodamage. To overcome such limits, we have recently demonstrated an Interferometric Cross-Polarization approach[17] that enables detection of single gold nanoparticles down to 5 nm diameter at excitation powers below 1 μW incident on the sample.

In this paper we provide a theoretical estimate and understanding of the sensitivity of the interferometric cross-polarized detection scheme by a quantitative comparison to the simplest case of direct detection of the transmitted light absorbed by an individual nanoparticle.[15] Against the commonly held notion that absorption-based detection schemes are more sensitive,[18] our analysis shows that, for the same signal-to-noise ratio, a scattering based interferometric detection scheme allows spherical 10 nm gold nanoparticles to be detected at near-infrared wavelengths with 2 orders of magnitude less incident optical power when operating above the plasmon resonance of the nanoparticle. We confirm this concept through the first experimental demonstration of detecting 10 nm gold nanoparticles at both visible and near-infrared wavelengths at sub-1 μW powers incident on the sample. This ability to achieve detection using extremely low power levels at near-infrared wavelengths holds considerable promise as an approach to exploit the potential of such small nanoparticles as biomarkers in living cells while causing minimal photodamage.

First let us consider the photon-limited sensitivity. Due to the discrete nature of photons, the precision with which one can detect an optical signal is fundamentally limited by shot noise.[19] A photon counter detecting, on average, N_s photons per time interval will, for many such intervals, yield a distribution of counts with a standard deviation $\sqrt{N_s}$, with this uncertainty being the shot noise. The resulting signal-to-noise ratio (SNR) in the background-free, shot-noise-limited case is then given by

$$\mathrm{SNR}_{\mathrm{shotnoise}} = \frac{N_s}{\sqrt{N_s}} = \sqrt{N_s} \tag{1}$$

which sets the classical limit for detecting changes in N_s.[20]

A molecule or nanoparticle with extinction cross-section σ_{ext} passing through a beam of linearly x-polarized light with area A results in a reduction of the incident photon flux N_{in} (in photons/sec) after the nanoparticle by $N_{ext} = \frac{\sigma_{ext}}{A} N_{in}$. Reducing the area A by focusing the incident light obviously increases the signal N_{ext}, however, one still has to detect this signal against the shot noise induced by the background of photons that have not interacted with the molecule or nanoparticle. For detection of a nanoparticle passing through the focus in transmission, as depicted in Figure 1a, the photon flux at the output of the collection lens and incident on the detector is given by

$$N_{out} = N_{in} - N_{ext} = \left(1 - \frac{\sigma_{ext}}{A}\right) N_{in} \tag{2}$$

This expression implicitly assumes that a plane polarized wave is incident on the scattering object, which is not strictly true for focused light.[21,22] However, instead of considering the extinction, absorption and scattering from first principle as done by Mohammadi and Agio,[22] we choose to follow this classical treatment as it enables a clearer discussion of SNRs.

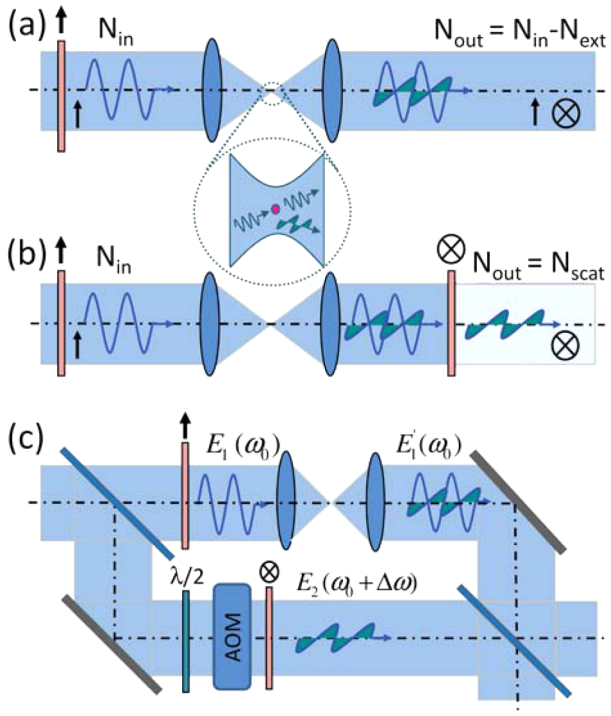

Figure 1. Focusing linear x-polarized light will create field components in all directions that are scattered or absorbed by a molecule or nanoparticle passing through the focus as shown schematically in the inset. (a) Direct detection in which both excitation light and light scattered by the nanoparticle are collected, with the signal originating from the extinction of light. (b) Cross-polarized detection scheme in which a polarizer with its transmission axis perpendicular to the incident linear polarization direction only transmits the scattered field components with a polarization perpendicular to the incident polarization in principle enabling background-free detection. (c) Interferometric Cross-Polarization detection scheme in which linear x-polarized light is split in a signal and reference branch. Interfering light from the signal-branch with a y-polarized reference that is frequency shifted by an Acousto-Optic Modulator(AOM) enables background-free detection of only y-polarized scattered photons by eliminating objective-induced depolarisation that in practice limits the scheme in (b).

To be detectable, the signal, N_{ext}, must exceed the uncertainty in the total photon count due to shot noise, $\sqrt{N_{out}}$. The SNR in this case is therefore given by

$$\mathrm{SNR}_{\mathrm{direct}} = \frac{N_{ext}}{\sqrt{N_{out}}} = \frac{\frac{\sigma_{ext}}{A} N_{in}}{\sqrt{\left(1 - \frac{\sigma_{ext}}{A}\right) N_{in}}} \approx \frac{\sigma_{ext}}{A} \sqrt{N_{in}} \tag{3}$$

in which the assumption is made that $\frac{\sigma_{ext}}{A} \ll 1$. Eq 3 enables us to estimate the photon flux needed for direct detection of the absorption by a single molecule in transmission. A single terrylene diimide (TDI) molecule, as used by Celebrano et al.[16] to demonstrate that it is possible to measure the absorption of a single molecule, is stated to have a cross section of 9×10^{-16} cm^{-2} at 632.8 nm when its electronic dipole matches the polarization of the incident light. For light focused by an objective with a numerical aperture (NA) of 1.45 this corresponds to $\frac{\sigma_{ext}}{A} \approx 4.0 \times 10^{-7}$, which shows that at least 6.1×10^{12} photons/s are needed to reach an SNR equal to one. At the wavelength used, this corresponds to a power of at least 1.9 μW impinging on a molecule with its absorption dipole

DOI: 10.1021/acsphotonics.5b00326
ACS Photonics 2015, 2, 1705−1711

moment aligned with the incident polarization if we assume a perfect detector that is able to count each photon. This number is consistent with the optical power of ∼100 μW used by Celebrano et al.[16] once optical losses (60%) and quantum efficiency (50%) of their detector are accounted for, assuming an SNR of 4.

From the above discussion, it can be seen that noise at the detector is dominated by the shot noise contribution from the background of photons that do not interact with the nanoparticle, represented by the unity term in eqs 2 and 3. As both the cross-section and A are fixed by the physical properties of the molecule and objective, respectively, the only available approach to increase SNR, thus, enabling detection at lower incident power levels, is the reduction of this background term. Here we consider background reduction through the use of a cross-polarized detection scheme that exploits the change in polarization direction of the light scattered from a nanoparticle. This effect arises because a tightly focused x-polarized beam yields a field in the focal plane that is no longer purely x-polarized but also contains y- and z-polarized components.[23] In the case of unperturbed focusing, these components in principle propagate to reconstruct an x-polarized far field. However, perturbation of the focal region due to a nanoparticle results in these components appearing in the far field, allowing a polarization-based detection scheme to be sensitive to only those photons that have interacted with the nanoparticle, as schematically depicted in Figure 1b.

The x-, y-, and z-components of the electrical field for a high NA oil-immersion objective with NA = 1.45 can in fact be calculated[23] and are displayed in Figure 2 for a filling factor of

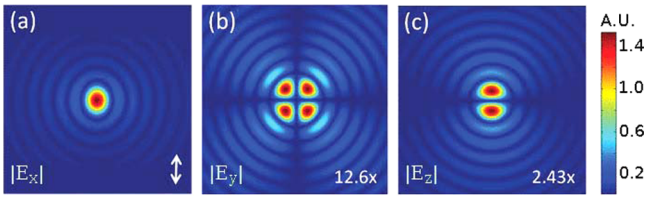

Figure 2. Shows the absolute value of the electric field in the x-, y-, and z-direction (from left to right) in the focus of a 1.45 NA objective when linear x-polarized light (λ = 632.8 nm) is focused to a diffraction limited spot. The incident polarization direction is indicated by the arrow in (a). The spatial extent of these images is 3 μm × 3 μm, and they are scaled to their maximum value using the multiplication factors indicated. The relative magnitude of this maximum field strength is used to provide a measure for the relative fraction γ of the incident linear x-polarized photons that are converted to x-, y-, and z-polarized photons, respectively.

2. Figure 2b and c are multiplied by 12.6 and 2.43, respectively, to enable comparison of the different field components using the same color scale. From this we see that the different field components have both a different strength as well as a different spatial distribution. To discuss SNRs, one is most interested in the ability to distinguish maxima, hence, we use the relative magnitude of the maximum field strength as a measure for the relative fraction γ of the incident linear x-polarized photons that are converted to x-, y-, and z-polarized photons, respectively. For an objective with NA = 1.45, we find $\gamma_{x\to x}$ = 0.8513, $\gamma_{x\to y}$ = 0.0054, and $\gamma_{x\to z}$ = 0.1433 showing that the field in the focal plane is dominated by the x-component, as would be expected. Note that as the incident and scattered field are collected by an objective, a similar conversion between polarization states will be induced upon collection. However, a lower NA collection objective with NA = 0.90 yields $\gamma_{x\to x}$ = 0.8973 showing that ignoring the polarization conversions for a lower NA air objective is a reasonable simplification.

To analyze the sensitivity of cross-polarized detection, we consider that a perfect polarizer is used to make the incoming light linearly x-polarized with a photon flux N_{in} passing this first polarizer as depicted in Figure 1b. Focusing this light will convert a fraction γ of the incident photon flux in x-, y- and z-polarized photons, respectively. This light, when scattered by a nanoparticle, will be collected by the collection objective leading to a scatterred photon flux in specific polarization states of

$$N_{\mathrm{scat,o}} = \gamma_{\mathrm{i}\to\mathrm{o}} \frac{\sigma_{\mathrm{scat}}}{A} N_{\mathrm{in}} \tag{4}$$

in which i and o represent the input and output polarization direction of interest, respectively, and σ_{scat} is the scattering cross-section. This change to the scattering cross-section reflects that we detect scattered photons in this detection scheme. The second perfect polarizer in Figure 1b will transmit light polarized in y, but block all x-polarized light. As a result, behind an ideal polarizer there will in principle be a photon flux of only $N_{\mathrm{out}} = N_{\mathrm{scat},y}$. In this case, the shot noise on a perfect detector behind the polarizer will be $\sqrt{N_{\mathrm{scat},y}}$ yielding a SNR of

$$\mathrm{SNR}_{\mathrm{crossed}} = \frac{N_{\mathrm{scat},y}}{\sqrt{N_{\mathrm{scat},y}}} = \sqrt{\gamma_{x\to y} \frac{\sigma_{\mathrm{scat}}}{A} N_{\mathrm{in}}} \tag{5}$$

From this equation we see that the required photon flux N_{in} to achieve the desired SNR becomes linear in $\frac{A}{\sigma_{\mathrm{scat}}}$ and no longer quadratic in $\frac{A}{\sigma_{\mathrm{ext}}}$, as was the case for direct detection (see eq 3), albeit with different cross sections. Despite this clear theoretical advantage, in practice, the SNR as given in eq 5 is not achievable using the detection scheme depicted in Figure 1b due to objective-induced depolarization, as we will explain below.

The extinction coefficient is an important figure of merit to consider in analyzing polarization microscopy.[24] The extinction coefficient is defined as the ratio of the intensity of light transmitted between parallel polarizers to that transmitted when polarizers are crossed. Ideally this extinction coefficient would be infinite; however, the image formation in wide-field microscopes prevent this even if the polarizers are perfect and in fact drops rapidly as the NA of the objectives is raised and typically a value of 1×10^{-3} is obtained.[24] This loss of extinction originates from the different transmission-coeffients and phase-shift experienced by s- and p-polarized rays as they pass through the optical interfaces under the large angles used in high-NA objectives.[25] In practice, one sees this phenomena manifest itself in the form of a Maltese cross at the output of a system[17,25] as drawn in Figure 1b. For an illumination objective of NA = 1.45 and a collection objective with NA = 0.90, this Maltese cross is clearly visible and one finds an extinction ratio of only 2.2×10^2 when this combination of objectives is placed between Glan−Thompson polarizers that have an extinction ratio of 5×10^5. As a result of this objective-induced depolarization effect, the SNR as given in eq 5 is therefore not achievable in wide-field microscopes, even in the case of perfect polarizers. However, this changes for single-point scanning confocal imaging systems as the polarization aberrations that occur at the exit pupil of the system have

DOI: 10.1021/acsphotonics.5b00326
ACS Photonics 2015, 2, 1705−1711

opposite phase in different quadrants in the exit pupil.[25] As a result, these aberrations cancel when overlapped with a reference beam to enable detection of the amplitude of the transmitted field instead of the intensity.[24,26] In fact, detecting the light's amplitude, in principle, allows infinite extinction ratios to be obtained as shown theoretically by Wilson and Tan.[27] In this measuring amplitude rather than intensity can be done by either using infinitely small pinholes or through interferometric detection of the light transmitted.[24]

Here we focus on the use of interferometric detection of the light scattered by the nanoparticle, as schematically depicted in Figure 1c. In this scheme, the polarizer in the frequency shifted reference branch is set to transmit E_y so that from the field exiting the collection objective, only E_y components that do not have antiphased equivalents (as occur for polarization aberrations in the imaging system) will interfere with the reference field to generate a signal at the modulation frequency, $\Delta\omega$. In the geometry displayed in Figure 1c, linear x-polarized light with a photon flux N_1 incident on the illumination objective is transformed by the scattering from a nanoparticle in the focus to

$$\mathbf{E}_1' = \begin{bmatrix} E_1 - E_{\mathrm{ext},x} \\ E_{\mathrm{scat},y} \end{bmatrix} \approx \begin{bmatrix} \sqrt{N_1} - \sqrt{N_{\mathrm{ext},x}} \\ \sqrt{N_{\mathrm{scat},y}} \end{bmatrix} \tag{6}$$

at the output of the collection objective in which $E_{\mathrm{ext},x}$ corresponds to the reduction of the x-polarized field as a result of both absorption and scattering. Note that, in the schematic diagram drawn in Figure 1c, the photons in both x- and y-polarization are incident on the detectors at the outputs of the interferometer as there is no polarizer present after the collection objective. We write the frequency shifted field in the reference branch as $\mathbf{E}_2(\omega + \Delta\omega)$, which is linearly y-polarized with a photon flux N_2. Assuming a 50/50 beam splitter, the resulting irradiance (I) on one of the perfect detectors at the output of the interferometer becomes

$$I_{\mathrm{det}} = \frac{\langle |\mathbf{E}_1' + \mathbf{E}_2|^2 \rangle}{2} = \frac{1}{2}\langle \mathbf{E}_1'^2 + \mathbf{E}_2^2 + 2\mathbf{E}_1'\cdot\mathbf{E}_2 \rangle \tag{7}$$

where $\langle\ \rangle$ denotes a time average over the response time of the detector. If we assume perfect overlap, this reduces for the case of orthogonal polarizations to

$$I_{\mathrm{det}} \approx \frac{1}{2}\langle E_1^2 + E_2^2 - 2E_1E_{\mathrm{ext},x}\cos(\phi_1) + 2E_2E_{\mathrm{scat},y}\cos(\Delta\omega + \phi_2)\rangle \tag{8}$$

in which we assume that $E_{\mathrm{ext},x}$, $E_{\mathrm{scat},y} \ll E_1,E_2$ and where ϕ_1,ϕ_2 corresponds to the phase difference between the interfering fields. From eq 8 we see that the small signal $E_{\mathrm{scat},y}$ corresponding to the y-component of the field scattered by the nanoparticle is interferometrically enhanced by the light in the reference branch, E_2. This enables us to select the optical flux in the reference branch sufficiently large so that the limiting factor is the shot noise of all the light incident on the detector and not the background electronic noise. Moreover, it shows that we can distinguish between scattered photons interfering with the incident light (E_1) and those interfering with the reference (E_2) as a result of the applied frequency modulation in the reference branch. If we maximize the signal by ensuring that $\phi_1 = \phi_2 = 0$ (constructive interference) and rewrite the measured irradiance in terms of photon flux we obtain

$$I_{\mathrm{det}} \approx \frac{N_1 + N_2}{2} - \sqrt{N_1}\sqrt{N_{\mathrm{ext},x}} + \sqrt{N_2}\sqrt{N_{\mathrm{scat},y}}\cos(\Delta\omega) \tag{9}$$

As the amount of light that interacts with a nanoparticle is small compared to N_1,N_2, the noise is given by $\sqrt{N_1 + N_2}$. With this approximation, the SNR becomes

$$\mathrm{SNR}_{\mathrm{inter}} \approx \frac{\sqrt{2N_2}\sqrt{N_{\mathrm{scat},y}}}{\sqrt{N_1 + N_2}} = \frac{\sqrt{2N_2}}{\sqrt{N_1 + N_2}}\sqrt{\gamma_{x\to y}\frac{\sigma_{\mathrm{scat}}}{A}N_1} \tag{10}$$

For the case where $N_2 \gg N_1$ as is the case here due to losses arising from overfilling the objective and total internal reflection occurring at the air−glass interface, this reduces to eq 5, albeit with an additional factor of $\sqrt{2}$. This factor results from our earlier assumption that we operate at constructive interference. The above equation demonstrates that the use of an interferometric cross-polarization scheme allows an SNR to be achieved equal to that of ideal cross-polarized detection, with perfect extinction and no objective-induced depolarisation. Comparing the given SNR expressions for direct and cross-polarized detection highlights the key advantage that in the cross-polarized interference case the required photon flux, N_{in}, becomes linear in $\frac{A}{\sigma_{\mathrm{scat}}}$ rather than quadratic in $\frac{A}{\sigma_{\mathrm{ext}}}$.

Direct detection and interferometric cross-polarized detection depend on distinct cross sections, thus one expects different wavelength dependence. Specifically relevant is the question which of these methods is more sensitive in the NIR. Fortunately, the general theory for scattering by spherical nanoparticles is well established, and these cross sections can be calculated using Mie theory.[21] In this theory, the interaction of a nanoparticle with light is characterized by the efficiencies of absorption and scattering resulting from their respective cross sections, σ_{abs} and σ_{scatt}. Both of these processes reduce the number of photons incident on the detector, leading to $\sigma_{\mathrm{ext}} = \sigma_{\mathrm{abs}} + \sigma_{\mathrm{scatt}}$ under the assumption that a plane wave is incident on the particle. In the limit of particles that are small compared to the wavelength, the absorption and scattering cross sections are given by[21]

$$\sigma_{\mathrm{abs}} = \frac{\pi^2 n_s}{\lambda} D^3 \mathrm{Im}\left(\frac{m^2 - 1}{m^2 + 2}\right) \tag{11}$$

and

$$\sigma_{\mathrm{scat}} = \frac{2\pi^5 n_s^4}{3\lambda^4} D^6 \left|\frac{m^2 - 1}{m^2 + 2}\right|^2 \tag{12}$$

where n_s is the refractive index of the medium, m is the ratio of complex refractive indices of the nanoparticle and the medium, and D is the diameter of the nanoparticle. These expressions allow analytical expressions to be derived for the required photon flux in the limit for spherical particles that are small compared to the wavelength showing that both approaches scale with D^{-6}.

To appreciate the wavelength dependence one has to introduce the dispersion of the complex refractive index of the particle. The extinction and scattering cross sections needed for this are calculated using Mie code published by Bohren and Huffman[21] (dashed lines) as well as in the small particle limit using eqs 11 and 12 (solid lines). The green and blue curve in Figure 3a show the calculated extinction and scattering cross-

DOI: 10.1021/acsphotonics.5b00326
ACS Photonics 2015, 2, 1705−1711

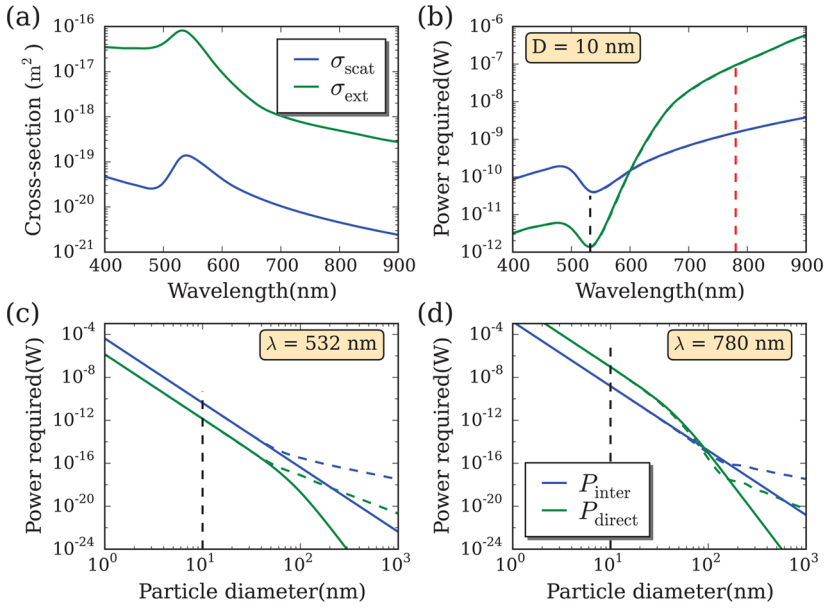

Figure 3. (a) Green and blue curves depict the extinction and scattering cross-section, respectively, for a 10 nm gold nanoparticle embedded in a medium with n = 1.5. (b–d) Green and blue curves display the optical power required to detect a gold nanoparticles with an SNR = 1 using direct detection and cross-polarized interferometric detection, respectively. From these curves the required power to achieve other SNRs can be calculated through multiplication by SNR^2. Dashed lines use Mie code by Bohren and Huffman[21] to calculate cross sections for gold spheres embedded in a medium with n = 1.5, while solid lines use cross sections in the small particle approximation. (b) Power required as a function of wavelength for a gold nanoparticle with D = 10 nm highlighting that for wavelengths above 600 nm two orders less optical power is required for interferometric cross-polarized detection. (c, d) Power required as a function of particle diameter for two typical wavelengths. Black and red dotted lines correspond to the wavelength and particle diameter used for the measurements presented in Figure 4.

section, respectively, for a 10 nm gold nanoparticle where the published Mie code overlaps with the curves obtained from eq 11 and eq 12. The refractive index values for gold have been taken from Johnson and Christy[28] and we assume that the particles are embedded in a homogeneous material with refractive index n_s = 1.5. The wavelength and particle-size dependence of the required optical power to achieve a SNR = 1 for both approaches are displayed in Figure 3b–d, in which the green and blue curves show the required optical power using direct and cross-polarized interferometric detection, respectively. These calculated powers follow from eqs 3 and 10, by multiplication with the photon energy. The spotsize, A, is treated as wavelength-dependent, with $\gamma_{x\rightarrow y}$ a constant with a value of 0.0054 as used previously. Figure 3b shows the required incident power to detect a single gold nanoparticle with a diameter of 10 nm and SNR = 1 as a function of wavelength, while Figure 3c and d show the diameter dependence for selected wavelengths in the visible and near-infrared. Powers needed to achieve other SNRs can be found from Figure 3b–d by multiplying the displayed values with SNR^2.

From these figures it is evident that for wavelengths in the NIR that are well above the plasmon resonance frequency of the spherical nanoparticle two orders less optical power is required in the case of cross-polarized interferometric detection (blue lines). This observation is counterintuitive as the commonly held notion is that for small nanoparticles absorption-based techniques are more sensitive than scattering based approaches, which is clearly not the case when operating above the plasmon resonance frequency. This increased sensitivity in the NIR for detecting spherical nanoparticles when using cross-polarized detection as opposed to direct detection is a clear consequence of the fact that for cross-polarized detection the required power to obtain a specific SNR scales linearly with $\frac{A}{\sigma_{scat}}$ rather than quadratically in $\frac{A}{\sigma_{ext}}$, as is the case for direct detection. So, despite the fact that at the plasmon resonance the scattering cross-section is 3 orders of magnitude lower than the extinction cross-section, as can be seen in Figure 3a, both show a similar reduction with wavelength and are 2–3 orders of magnitude lower in the NIR. As a result of the linear versus quadratic dependence of the required optical power this, hence, leads to the observed enhanced sensitivity of roughly 2 orders of magnitude for a cross-polarized scattering based approach at λ = 780 nm compared to direct detection. Interestingly enough, this advantage for cross-polarized interferometric detection only applies to particles that are well within the small particle approximation as we can see from the crossover visible in Figure 3d at a diameter of 80 nm. A similar trend is found for silver nanoparticles that have a lower plasmon resonance frequency, although for those it is beneficial to use interferometric cross-polarized detection at all displayed wavelengths and, in fact, 4 orders less optical power is needed in the NIR. It is important to realize that the sensitivity for interferometric cross-polarized in the NIR is below that of direct detection when working at the plasmon resonance, as can be seen directly from Figure 3b by comparing the minimum powers needed at 532 and 780 nm, respectively.

To provide experimental evidence that it is indeed possible to detect 10 nm spherical gold nanoparticles at ultralow excitation powers by a scattering based approach we imaged single gold nanoparticles with a diameter of 10 ± 1 nm at both visible (λ = 532 nm) and NIR (λ = 780 nm) wavelengths using an excitation power of less than 1 μW incident on the sample. For the NIR measurements we used a laser-diode emitting at 780 nm (Aixiz, A-780–10–3.2) and further details on sample preparation and the experiment can be found elsewhere.[29] The

DOI: 10.1021/acsphotonics.5b00326
ACS Photonics 2015, 2, 1705–1711

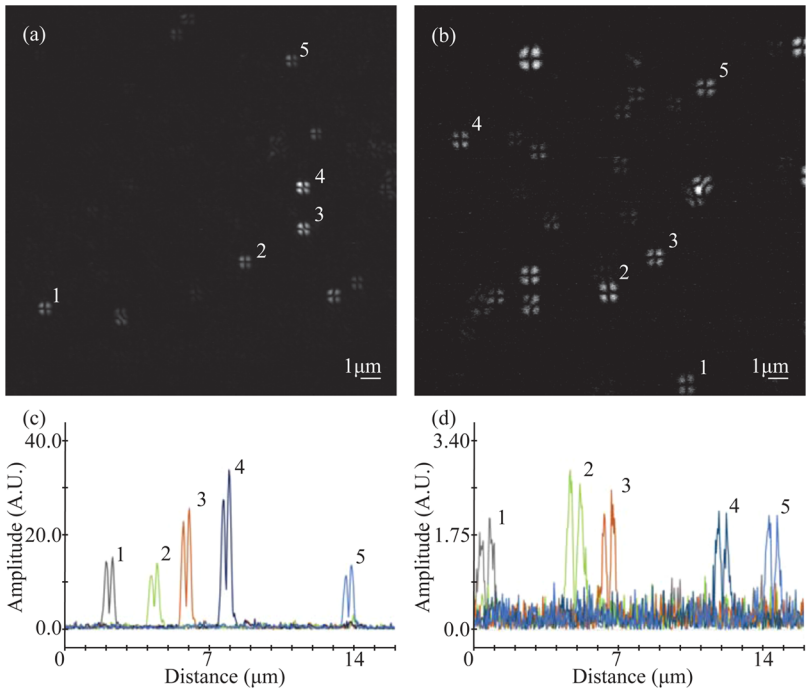

Figure 4. Interferometric cross-polarization imaging of 10 ± 1 nm diameter gold nanoparticles at visible and near-infrared excitation. The detected amplitude of the scattered light is shown for particles excited by (a) λ = 532 nm, with a power of 1.2 and 9.5 μW in the signal and reference branch, respectively. (b) λ = 780 nm, with a power of 1.2 and 3.2 μW in the signal and reference branch, respectively. With a filling factor of 2, this in both cases corresponds to a power of less than 1 μW incident on the sample. The spatial extent of the images is 18.4 μm × 18.4 μm, for the fast and slow axis, respectively, with a 1.5 ms pixel dwell time and a lock-in integration time of 366 μs. Vertical line-traces across the center of the two left-hand lobes for five selected particles to highlight the SNR obtained for (c) λ = 532 nm and (d) 780 nm.

cross-polarized amplitude image for λ = 532 and 780 nm is shown in Figure 4a and b, respectively. In this the observed amplitude distribution of each individual nanoparticle in first approximation resembles the expected E_y field component displayed in Figure 2b, as discussed by Hong et al.[17] The exact image formation is, however, slightly more complex, as it results from interference with the reference. For these images collected at the focal plane, the interference primarily reduces the amplitude of the sidelobes visible in Figure 2b.[29]

To highlight the SNR obtained, Figure 4c,d shows line-traces across the center of the two left-hand lobes of the patterns visible for five selected nanoparticles at λ = 532 and 780 nm, respectively. For clarity, high features arising from other particles on the same line have been removed where needed. These results were obtained using a power of 1.2 μW in the signal branch in both cases. With a filling factor of 2, this corresponds to a power of less than 1 μW incident on the sample, demonstrating that it is possible to detect single nanoparticles with a good SNR for ultralow excitation powers for both visible and NIR wavelengths. Note that at these excitation powers it would not be possible to image these particles with the obtained SNR using the direct detection scheme depicted in Figure 1b, as can be determined from the required optical powers depicted in Figure 3b. To achieve the SNR of **4** seen in Figure 4d would require 2 μW incident on the sample, which exceeds the power used here. Unfortunately, it is difficult to directly compare the SNRs obtained for λ = 532 nm and λ = 780 nm against our modeling due to practical limitations. The sample preparation for the experiments shown has been identical, yet different illumination fibers had to be used and in the NIR the SNR is severely affected by mode-hopping noise of the laser used,[30] which completely dominates the noise visible in Figure 4d. It is worth noting that this type of noise is not a fundamental limitation for the technique, as amplitude noise of this type can be suppressed by using a more stable laser diode or through balanced detection of the interferometric signal as we recently demonstrated.[31]

To conclude, we have shown that the orthogonality of the light in the two polarization branches of the interferometer ensures that only light that has interacted with a nanoparticle passing through the focus will be interferometrically enhanced. This results in a SNR corresponding to background-free shot noise-limited detection of spherical nanoparticles at optical powers significantly lower than would be possible in direct detection of transmitted light when operating above the plasmon resonance frequency, enabling the use of low optical powers incident on the sample reducing associated photo-damage and phototoxicity. We have shown this experimentally by demonstrating that single gold nanoparticles with a diameter of 10 ± 1 nm can be detected using cross-polarized detection with a good SNR using an illumination power of less than 1 μW incident on the sample at both visible and NIR wavelengths. The use of an interferometer combined with single-point imaging, moreover, enables the removal of polarization aberrations resulting from the imaging system enabling polarization measurements with high spatial resolution and low illumination power in living cells. Our preliminary work toward cell imaging indicates that the signal levels resulting from the cell interior in interferometric cross-polarization imaging are below those obtained for 10 nm gold nanoparticles provided that sufficient care is taken during sample preparation to reduce edge birefringence of the cell surface. This highlights the potential of this approach to localize single gold nanoparticles in living cells with high spatial resolution in the

DOI: 10.1021/acsphotonics.5b00326
ACS Photonics 2015, 2, 1705−1711

wavelength regime where absorption by biomolecules and water is low.

AUTHOR INFORMATION

Corresponding Author

*E-mail: h.gersen@bristol.ac.uk.

Notes

The authors declare no competing financial interest.

ACKNOWLEDGMENTS

This work was funded in part by the Biotechnology and Biological Sciences Research Council through a Technology Development Research Initiative (Grant Ref.: BB/F004494/1) and carried out with the support of the Bristol Centre for Nanoscience and Quantum Information. I.D.L. acknowledges the support of EPSRC via an Advanced Research Fellowhip (Grant Ref.: EP/E054536/1). We would furthermore like to thank Nick and Susan Woollacott who kindly funded an essential part of the equipment used in this research.

REFERENCES

(1) Stender, A. S.; Marchuk, K.; Liu, C.; Sander, S.; Meyer, M. W.; Smith, E. A.; Neupane, B.; Wang, G.; Li, J.; Cheng, J.-X.; Huang, B.; Fang, N. Single cell optical imaging and spectroscopy. *Chem. Rev.* **2013**, *113*, 2469−2527.

(2) Yildiz, A.; Tomishige, M.; Vale, R. D.; Selvin, P. R. Kinesin walks hand-over-hand. *Science* **2004**, *303*, 676−678.

(3) Lommerse, P. H. M.; Blab, G. A.; Cognet, L.; Harms, G. S.; Snaar-Jagalska, B. E.; Spaink, H. P.; Schmidt, T. Single-molecule imaging of the H-ras membrane-anchor reveals domains in the cytoplasmic leaflet of the cell membrane. *Biophys. J.* **2004**, *86*, 609−616.

(4) Welsher, K.; Yang, H. Multi-resolution 3D visualization of the early stages of cellular uptake of peptide-coated nanoparticles. *Nat. Nanotechnol.* **2014**, *9*, 198−203.

(5) Vallée, R.; Tomczak, N.; Gersen, H.; Van Dijk, E. M. P. H.; García-Parajó, M. F.; Vancso, G. J.; Van Hulst, N. F. On the role of electromagnetic boundary conditions in single molecule fluorescence lifetime studies of dyes embedded in thin films. *Chem. Phys. Lett.* **2001**, *348*, 161−167.

(6) Weiss, P. S. Nobel Prizes for Super-Resolution Imaging. *ACS Nano* **2014**, *8*, 9689−9690.

(7) Donnert, G.; Eggeling, C.; Hell, S. W. Major signal increase in fluorescence microscopy through dark-state relaxation. *Nat. Methods* **2007**, *4*, 81−86.

(8) Ortega-Arroyo, J.; Kukura, P. Interferometric scattering microscopy (iSCAT): new frontiers in ultrafast and ultrasensitive optical microscopy. *Phys. Chem. Chem. Phys.* **2012**, *14*, 15625−15636.

(9) Müller-Reichert, T.; Verkade, P. *Correlative Light and Electron Microscopy*; Academic Press: New York, 2012; Vol. *111*.

(10) Huang, X.; Jain, P. K.; El-Sayed, I. H.; El-Sayed, M. A. Gold nanoparticles: interesting optical properties and recent applications in cancer diagnostics and therapy. *Nanomedicine* **2007**, *2*, 681−693.

(11) Zijlstra, P.; Orrit, M. Single metal nanoparticles: optical detection, spectroscopy and applications. *Rep. Prog. Phys.* **2011**, *74*, 106401.

(12) Yurt, A.; Daaboul, G. G.; Connor, J. H.; Goldberg, B. B.; Ünlü, M. S. Single nanoparticle detectors for biological applications. *Nanoscale* **2012**, *4*, 715−726.

(13) Chong, S.; Min, W.; Xie, X. S. Ground-state depletion microscopy: detection sensitivity of single-molecule optical absorption at room temperature. *J. Phys. Chem. Lett.* **2010**, *1*, 3316−3322.

(14) Gaiduk, A.; Yorulmaz, M.; Ruijgrok, P. V.; Orrit, M. Room-temperature detection of a single molecules absorption by photothermal contrast. *Science* **2010**, *330*, 353−356.

(15) Kukura, P.; Celebrano, M.; Renn, A.; Sandoghdar, V. Single-molecule sensitivity in optical absorption at room temperature. *J. Phys. Chem. Lett.* **2010**, *1*, 3323−3327.

(16) Celebrano, M.; Kukura, P.; Renn, A.; Sandoghdar, V. Single-molecule imaging by optical absorption. *Nat. Photonics* **2011**, *5*, 95−98.

(17) Hong, X.; van Dijk, E. M. P. H.; Hall, S. R.; Götte, J. B.; van Hulst, N. F.; Gersen, H. Background-free detection of single 5 nm nanoparticles through interferometric cross-polarization microscopy. *Nano Lett.* **2011**, *11*, 541−547.

(18) Van Dijk, M. A.; Tchebotareva, A. L.; Orrit, M.; Lippitz, M.; Berciaud, S.; Lasne, D.; Cognet, L.; Lounis, B. Absorption and scattering microscopy of single metal nanoparticles. *Phys. Chem. Chem. Phys.* **2006**, *8*, 3486−3495.

(19) Freise, A.; Strain, K. A. Interferometer Techniques for Gravitational-Wave Detection. *Living Reviews in Relativity* **2010**, *13*.10.12942/lrr-2010-1

(20) Caves, C. M. Quantum-mechanical noise in an interferometer. *Phys. Rev. D: Part. Fields* **1981**, *23*, 1693.

(21) Bohren, C. F.; Huffman, D. R. *Absorption and Scattering of Light by Small Particles*; John Wiley & Sons: New York, 2008.

(22) Mohammadi, A.; Agio, M. Light scattering under nanofocusing: Towards coherent nanoscopies. *Opt. Commun.* **2012**, *285*, 3383−3389.

(23) Novotny, L.; Hecht, B. *Principles of Nano-Optics*; Cambridge University Press: New York, 2012.

(24) Higdon, P.; Juškaitis, R.; Wilson, T. The effect of detector size on the extinction coefficient in confocal polarization microscopes. *J. Microsc.* **1997**, *187*, 8−11.

(25) Shribak, M.; Inoue, S.; Oldenbourg, R. Polarization aberrations caused by differential transmission and phase shift in high-numerical-aperture lenses: theory, measurement, and rectification. *Opt. Eng.* **2002**, *41*, 943−954.

(26) Wilson, T.; Juškaitis, R. On the extinction coefficient in confocal polarization microscopy. *J. Microsc.* **1995**, *179*, 238−240.

(27) Wilson, T.; Tan, J. B. Finite sized coherent and incoherent detectors in confocal microscopy. *J. Microsc.* **1996**, *182*, 61−66.

(28) Johnson, P. B.; Christy, R. W. Optical Constants of the Noble Metals. *Phys. Rev. B* **1972**, *6*, 4370−4379.

(29) Miles, B. T.; Hong, X.; Gersen, H. On the complex point spread function in interferometric cross-polarisation microscopy. *Opt. Express* **2015**, *23*, 1232−1239.

(30) Fukuma, T.; Kimura, M.; Kobayashi, K.; Matsushige, K.; Yamada, H. Development of low noise cantilever deflection sensor for multienvironment frequency-modulation atomic force microscopy. *Rev. Sci. Instrum.* **2005**, *76*, 053704.

(31) Robinson, E. C.; Trägårdh, J.; Lindsay, I. D.; Gersen, H. Balanced detection for interferometry with a noisy source. *Rev. Sci. Instrum.* **2012**, *83*, 063705.

DOI: 10.1021/acsphotonics.5b00326
ACS Photonics 2015, 2, 1705−1711